Design of laser-aided diagnostics for the negative hydrogen ion source SPIDER

2012 JINST 7 C04016

(http://iopscience.iop.org/1748-0221/7/04/C04016)

PUBLISHED BY IOP PUBLISHING FOR SISSA MEDIALAB

RECEIVED: *November 22, 2011*
ACCEPTED: *March 13, 2012*
PUBLISHED: *April 20, 2012*

15th INTERNATIONAL CONFERENCE ON LASER AIDED PLASMA DIAGNOSTICS,
OCTOBER 13–19, 2011
JEJU, KOREA

Design of laser-aided diagnostics for the negative hydrogen ion source SPIDER

R. Pasqualotto

Consorzio RFX, Associazione EURATOM-ENEA sulla Fusione,
Corso Stati Uniti 4, 35127 Padova, Italy

E-mail: roberto.pasqualotto@igi.cnr.it

ABSTRACT: ITER nuclear fusion experiment requires additional heating via neutral beams by means of two injectors, delivering 16.5 MW each, up to one hour. This power level results from the neutralization of negative deuterium ions generated by an RF source and accelerated to 1 MeV. Such specifications have never been simultaneously achieved so far and therefore a test facility is being constructed at Consorzio RFX, to demonstrate the feasibility of a prototype neutral beam injector. The facility will host two experimental devices: SPIDER, a 100 kV negative hydrogen/deuterium RF source, full size prototype of the ITER source, and MITICA, a prototype of the full ITER injector. SPIDER will be devoted to optimize the extracted negative ion current density and its spatial uniformity and to minimize the co-extracted electron current. Negative hydrogen is mainly produced by conversion of hydrogen particles at the cesium coated surface of the plasma grid. The interplay of these two species is fundamental to understand and optimize the source performance. Two laser-aided diagnostics play an important role in measuring the negative hydrogen and cesium density: cavity ring down spectroscopy and laser absorption spectroscopy. Cavity ring down spectroscopy will use the photo-detachment process to measure the absolute line-of-sight integrated negative ion density in the extraction region of the source. Laser absorption spectroscopy will be employed to measure the line integrated neutral cesium density, allowing to study the cesium distribution in the source volume, during both the plasma and the vacuum phases. In this paper, the design of the laser-aided diagnostic systems on SPIDER is presented, supported by a review of results obtained in other operating experiments.

KEYWORDS: Ion sources (positive ions, negative ions, electron cyclotron resonance (ECR), electron beam (EBIS)); Plasma diagnostics - charged-particle spectroscopy; Plasma diagnostics - interferometry, spectroscopy and imaging

doi:10.1088/1748-0221/7/04/C04016

2012 JINST 7 C04016

Contents

1 Development of neutral beam injectors for ITER

ITER, the nuclear fusion experimental reactor under construction, is expected to produce 0.5 GW of fusion power, steady state. Depending on the operating scenario, ITER requires an additional power of 33–50 MW from neutral beam injectors (NBI); such power can be provided by two or three accelerators, each delivering to ITER 16.5 MW; the accelerated negative ion current should be 40 A and the accelerating voltage 1 MV [1]. Negative hydrogen or deuterium ions are used, because, unlike positive ions, they exhibit constant neutralisation efficiency up to 1 MeV. The pulse should last more than 1000 s and the beam should have a divergence lower than 7 mrad. These requirements have never been achieved simultaneously so far and therefore, in order to minimize the risks and the time to provide ITER with reliable NBIs, the need of a robust experimental demonstration and of the optimization of critical components and systems, has led to the construction of a neutral beam test facility to be hosted at Consorzio RFX in Italy, comprising two experimental test stands, SPIDER and MITICA [2]. SPIDER will optimize a full size negative ion source to full power and pulse length in H^- or D^-. Its mission is to demonstrate the capability to create and extract a current of D^- (H^-) up to approximately 50 A (60 A) and to accelerate it to 0.1 MeV, with a beam uniformity of $\pm 10\%$ and a coextracted electron fraction (e^-/D^-) < 1. The second test stand, MITICA, is the prototype of the ITER injector, which aims at developing all the knowledge and technologies to guarantee the successful operation of the two injectors to be installed on ITER.

SPIDER, represented in figure 1, produces a beam which is made up of an array of 1280 beamlets, generated by a set of accelerating grids with an equal amount of apertures, distributed over an area of $1.5 \times 0.6\,m^2$, with a total aperture area on the plasma grid, the first facing the plasma source, of $0.2\,m^2$. SPIDER beam source represents the final step of a development path, begun at IPP Garching, where the concept was proposed and extensively experimented on a series

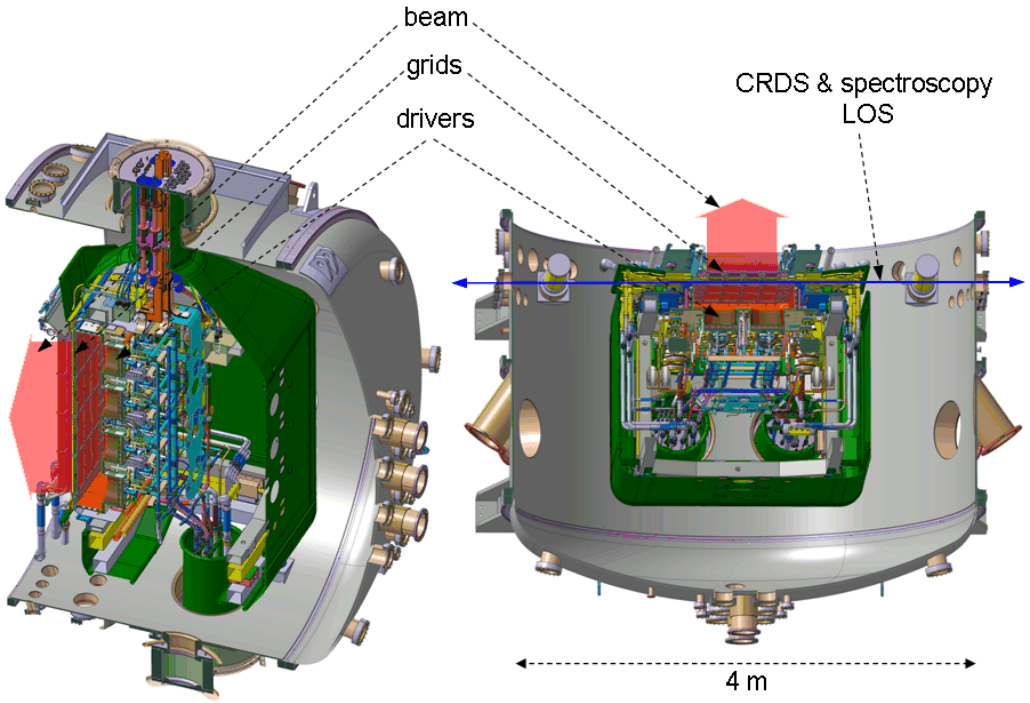

Figure 1. 3D model of SPIDER: vertical (*left*) and horizontal (*right*) section.

of small scale RF sources and where a half size source is under construction [3]. Although IPP RF sources have made substantial progress towards ITER's requirements, there are still open issues, like homogeneity of a large RF source, long pulse stability and suppression of electrons, which are required to be solved on a full scale source.

2 H^- production in the RF source

In the SPIDER RF source, plasma is generated inside eight cylindrical RF drivers, operating at 1 MHz and delivering 800 kW total power. From here, the plasma expands into a common rectangular case, called the expansion region, towards a set of grids on the opposite side, which serve as the extraction/acceleration system. This is made of a plasma grid (PG) biased at -100 kV, slightly positive with respect to the source case, followed by the extraction grid at -88 kV and finally by the grounded grid at ground potential. H^- or D^- ions are generated mainly by a cesium assisted surface process: cesium is evaporated inside the source and it coats the internal molybdenum surface reducing its work function to about 2.2–2.5 eV [4]; neutral and positive hydrogen atoms hitting the PG are then more easily converted into negative ions, which, with a binding energy of the additional electron of 0.75 eV, have a survival length as short as few cm. Only negative ions generated at the PG have then a chance to be extracted. A H^- density of about 10^{17} m^{-3} is produced there, capable to sustain the required H^- (D^-) current density of 280 Am^{-2} (200 Am^{-2}). This thin region in front of the PG is called extraction region and it is separated from the expansion region by a magnetic filter field, parallel to the PG, that reduces the electron density and temperature from respectively 10^{18} m^{-3} and 10 eV to 10^{17} m^{-3} and 2 eV, reducing the negative ion destruction by electron strip-

ping. An additional plate (bias plate), framing the PG and sitting at the potential of the source case, contributes to reduce the current of co-extracted electrons. The other process responsible for H^- production, the volume process of dissociative attachment of the vibrationally excited hydrogen molecules, is ten times less efficient at the typical source pressure of 0.3 Pa, which has been chosen sufficiently low to reduce the beam attenuation in the extraction and acceleration region.

The H^- production mechanism thus described can strongly depend on the geometry of the source (discrete drivers and magnetic field profile), on the cesium dynamics and on the still little known and certainly hardly controllable mechanisms that determine the work function at the PG surface, on the relative contributions of neutral and positive ions in producing H^- and on the H^- transport towards the apertures of the PG, from which acceleration starts. All these mechanisms can have a strong spatial dependence across the PG surface, which would reflect into a non uniformity in H^- production. How this correlates with the beam non uniformity is still under investigation, as the beam properties are mainly determined by the parameters at the meniscus, where it is practically impossible to perform any measurement. As best estimate, efforts have focused on measuring all relevant parameters, starting from few mm out of the PG surface: this criterion has been applied in designing the diagnostics for SPIDER.

3 SPIDER diagnostics

SPIDER has been equipped with a set of diagnostics that, besides supporting a safe and controlled operation, allow to fully characterise the beam in terms of uniformity and divergence and the source with particular attention to the H^- production, cesium dynamics and overall plasma characteristics [5–7]. This is achieved with a set of complementary diagnostics, with their specific advantages and limitations; e.g. for beam uniformity and divergence, a high spatial resolution instrumented calorimeter working only on short pulses is complemented by beam emission spectroscopy and visible tomography, while in the source the negative ion density is measured by both emission spectroscopy, easier to perform, but more difficult to interpret, and by cavity ring down spectroscopy (CRDS), which provides a direct absolute measurement, but is more difficult to operate and maintain. In addition, measurements of the beam profile are correlated to measurements of key plasma parameters inside the source, across the large grid area in order to investigate possible local effects.

The beam source is mainly diagnosed by current measurements, thermocouples, which provide the heat load distribution, and emission spectroscopy which, supported by suitable interpretative models, can provide line integrated measurements of electron temperature, density of electrons, negative ions, cesium, neutral hydrogen. Spectroscopy also monitors the amount of impurities. It is complemented by an array of electrostatic probes, which provide spatial profiles of electron temperature and density, ion density and plasma potential in front of the PG and bias plate. However probes and thermocouples are difficult to operate and maintain because they are at high potential and the signals are extracted from the grounded vacuum vessel through a high voltage bushing, with an intense RF background. Optical diagnostics are preferred and, in particular, laser aided methods like CRDS and laser absorption spectroscopy have been found useful for measurements of some critical parameters at IPP RF sources. Such diagnostics will be implemented also on SPIDER, as described in the following sections.

2012 JINST 7 C04016

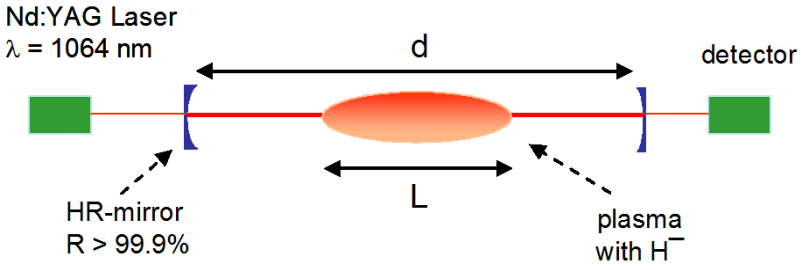

Figure 2. Schematic of the CRDS setup.

4 Cavity ring down spectroscopy

CRDS is based on the observation of the intensity decay of a laser light pulse trapped in a cavity formed by two very high reflectivity mirrors. It has been widely used in the past two decades in several applications and appreciated for its high sensitivity due to the multipass optical path [8]. First use on a large-area RF industrial plasma reactor was reported in [9], with 1.2 m long cavity. It has been recently introduced as a reliable, absolute, self-calibrated measurement of the line-of-sight integrated H^- density, insensitive to electromagnetic interference and magnetic field, at the IPP RF sources [10] and at the LHD negative neutral beam test facility [11, 12].

CRDS uses the photodetachment process:

$$H^- + h\nu \rightarrow H + e \tag{4.1}$$

where H^- ions are converted to neutrals when the additional electron is stripped off by photon absorption [13]. This reaction has a broadband cross-section, peaking at about 1.5 eV and extending down to the threshold value given by the binding energy of the additional electron. A Nd:YAG laser at 1064 nm well sets near the peak, with a cross-section $\sigma_{H^-} = 3.5 \times 10^{-21}$ m^2, but also a second harmonic Nd:YAG could be used, with a slightly lower cross section and the advantage of being visible. In either case spurious absorption contributions might pollute the measurement: at 532 nm additional absorption might occur by H_2^+ ions, while at 1064 nm absorption by cesium dimers, Cs_2, has been assumed as possible explanation of an observed spurious signal [10].

In the typical CRDS setup (figure 2) a laser pulse is injected into a cavity formed by two highly reflective mirrors (reflectivity $R > 99.99\%$). The light reflects back and forth inside the cavity and the small fraction leaking through one of the cavity mirrors, monitored by a suitable detector, decays according to a simple exponential function of the form:

$$I(t) = I_0 \cdot e^{-t/\tau} \quad \text{with} \quad \tau = \frac{d}{c(1 - R + \alpha \cdot L)} \tag{4.2}$$

where R is the mirror reflectivity, d the cavity length, I_0 is the initial intensity, c is the light speed, t is time, α is the absorption coefficient of some absorbing species in the cavity and L the length of the beam path through this absorbing medium in a single pass. In our case the decay constant is a direct measurement of the absorption by H^- in the cavity, from which its average density is derived:

$$\bar{n}_{H^-} = \frac{1}{\sigma_{H^-}} \cdot \frac{d}{c \cdot L} \cdot \left(\frac{1}{\tau} - \frac{1}{\tau_0} \right) \tag{4.3}$$

where τ_0 is the intrinsic absorption time without plasma and τ with plasma.

In IPP sources and in SPIDER, CRDS complements emission spectroscopy in measuring the negative ion density. Emission spectroscopy employs the H_α/H_β line ratio method to estimate the H^- density. It has the advantages of being easily implemented and also of being insensitive to electromagnetic interference. However data analysis is based on a collisional radiative model dependent on plasma parameters and cross sections, so that relative estimates of H^- density can be obtained with 20% accuracy and absolute ones with up to 40% [14]. At IPP a third diagnostic, laser photodetachment with a movable Langmuir probe, measures the n_{H^-}/n_e profile, from which the H^- density profile is derived, after independently measuring the n_e profile with Langmuir probes [15]. Langmuir probes are however disturbed by the noisy environment and while still relatively easy to be inserted in IPP sources, because they are in air, though at high voltage, it is very difficult to scan a probe inside the SPIDER source, because the whole source lies in vacuum. For this reason laser photodetachment has not been considered for SPIDER.

CRDS has also some disadvantages that might reduce its reliability for routine operation: difficulty in maintaining good cavity alignment and possible mirror transmission deterioration because of coating by impurities inside the vacuum tank. However the successful operations at IPP and at the LHD negative neutral beam test facility have demonstrated its capabilities in this application. At IPP [10], with $\lambda = 1064$ nm, $d = 1.2$ m and $L = 0.25$ m, and with $\tau_0 = 38\,\mu$s, the dynamic range of the system could cover the actual H^- density range from 10^{15}–10^{17} m^{-3} in front of the PG, with a repetition rate of 4 Hz. Main error contribution is the uncertainty on L, estimated about 15%, resulting in an overall accuracy less than 20%. However the uncertainty on L is a systematic error contribution which affects just the absolute value of the average density defined in (4.3), but not the measured line integrated density. A clear dependence on the RF power and a linear correlation with the extracted H^- current density were found, with better extraction efficiency at lower source pressure. The CRDS system in the arc source at LHD [11, 12], also with $\lambda = 1064$ nm and with a similar geometry, $d = 1.57$ m and $L = 0.35$ m, has higher $\tau_0 = 115\,\mu$s and exponential fit accuracy was 1%, in line with IPP results, at 20 Hz repetition rate. In the LHD source, H^- density is linearly related to both the arc power and the extracted H^- current. Here the cavity mirrors could be translated in order to scan the distance to the PG from 5 to 17 mm: a spatial profile was measured with a resolution of 2 mm, given by the beam diameter.

4.1 CRDS on SPIDER

CRDS on SPIDER [16] will be similar to the two systems already in operation cited above, except for the larger size, $d = 4.3$ m, $L = 0.56$ m, and the longer plasma pulse. The two cavity mirrors are mounted as vacuum windows on the same adjustable commercial flange used also by other CRDS setups, installed on opposite sides of the SPIDER vacuum vessel and isolated by gate valves when not operational, to preserve the mirrors from impurity deposition. The cavity layout is illustrated in figure 3 and figure 4. The cavity can be installed on a choice of horizontal lines of sight (LOS) parallel to the PG, at different heights to measure the H^- density vertical uniformity and at different distances from the PG surface to measure the H^- density profile perpendicular to the grid. This spatial profile cannot be measured with a continuous scan, but at fixed positions, as each possible LOS is identified by a pair of opposite 10 mm diameter holes on the source lateral wall and supporting structure; besides, the bias plate allows only few LOSs through it, in the horizontal slots where it is cut (see figure 3 and figure 5). Figure 5 shows the full set of 9 pairs of opposite viewports

2012 JINST 7 C04016

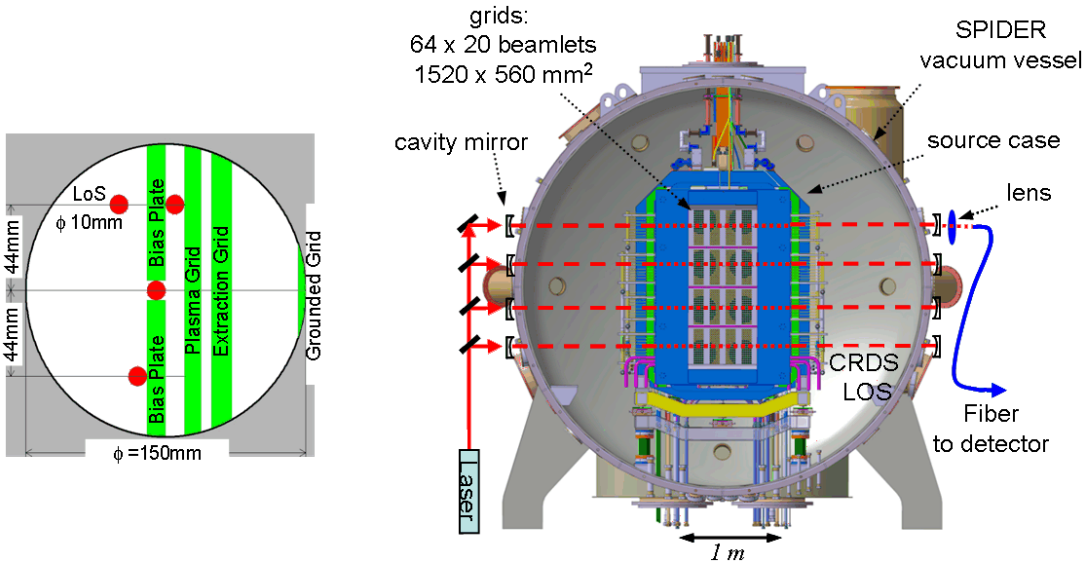

Figure 3. Layout of the CRDS LOSs. *Right*: front view, LOSs crossing the 4×4 beamlet groups at different heights and with cavity mirrors on the vessel ports. *Left*: side view of the viewport, with apertures (circles) for LOSs at 5, 15, 25 and 35 mm from the plasma grid.

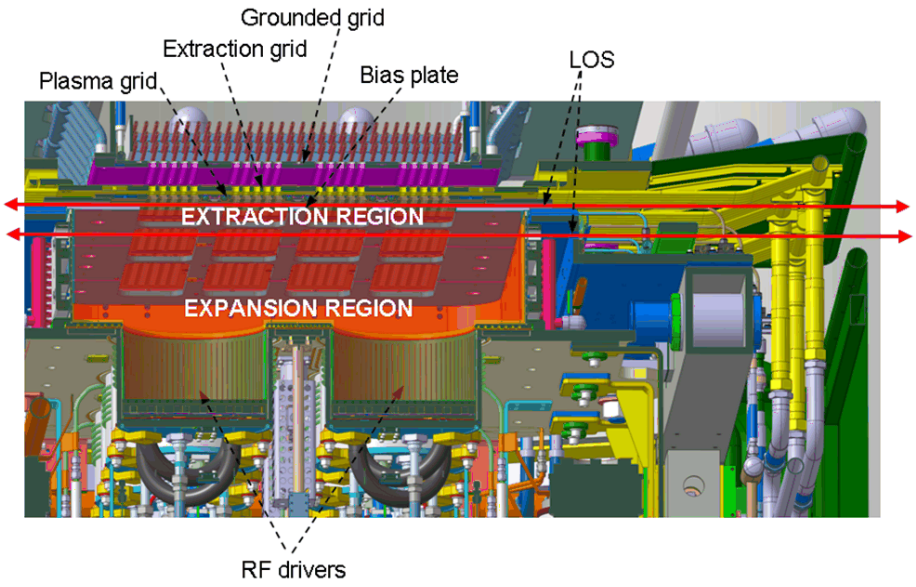

Figure 4. Horizontal section of the SPIDER source showing the CRDS laser beam paths between PG and bias plate and at 35 mm from the PG.

used for spectroscopic horizontal LOSs parallel to the PG and the LOSs projection onto the PG and its rows of apertures. The four 150 mm diameter clear aperture flanges, one at the centre of each horizontal grid segment, can accommodate four LOSs at 5, 15, 25 or 35 mm from the PG, best suited for CRDS. The design still leaves the option to use a single cavity, alternatively installing it on the available LOSs, or to split the available laser beam onto multiple beams with beamsplitters and install parallel CRDS cavities, running simultaneously. Figure 6 illustrates the plant view of

2012 JINST 7 C04016

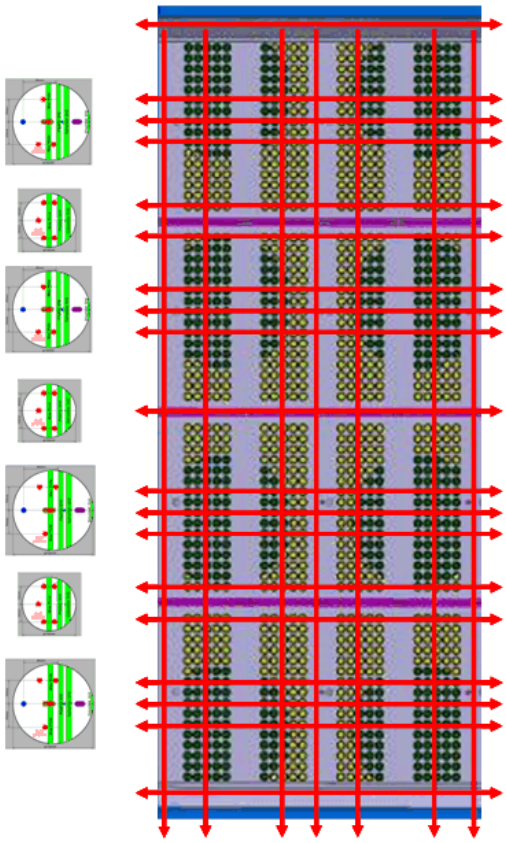

Figure 5. Portholes on the side of the beam source vessel, hosting the emission spectroscopy and the CRDS LOSs (*left*) and positions of the LOSs with respects to the plasma grid (*right*). The footprint of the eight drivers is represented on the grid.

the test facility, with the laser installed just outside the biological shield containing SPIDER and the beam properly steered and focused inside the cavity, with the lens focal length properly chosen to avoid vignetting from the source case stops. The CRDS signal is collected by an $f = 25$ mm lens and fed into a 1 mm diameter optical fibre which runs outside the bioshield to the detection and acquisition system, located in a separate room. Avoiding any electrical component inside the bioshield should minimise the electromagnetic interference at 1 MHz, still observed at IPP though following the same approach.

4.2 CRDS prototype for SPIDER

A benchtop prototype of the CRDS diagnostic for SPIDER has been installed and operated, to select and test the diagnostic components, to develop a suitable alignment procedure and to investigate the sensitivity of the cavity to misalignments. The layout is sketched in figure 7, while in figure 8 a photo of the setup is reproduced, with the optical path overlapped. The selected Nd:YAG laser at $\lambda = 1064$ nm runs at 10 Hz, with 6 mm beam diameter and pulse energy and duration tunable from 330 mJ/5 ns to 25 mJ/12 ns. The cavity was made of two commercial mirror mounts serving also as vacuum flanges of a 4.3 m long vacuum tube. The cavity was operated both in vacuum and in air, but without plasma production so that only the reference ring down time τ_0 could be measured.

2012 JINST 7 C04016

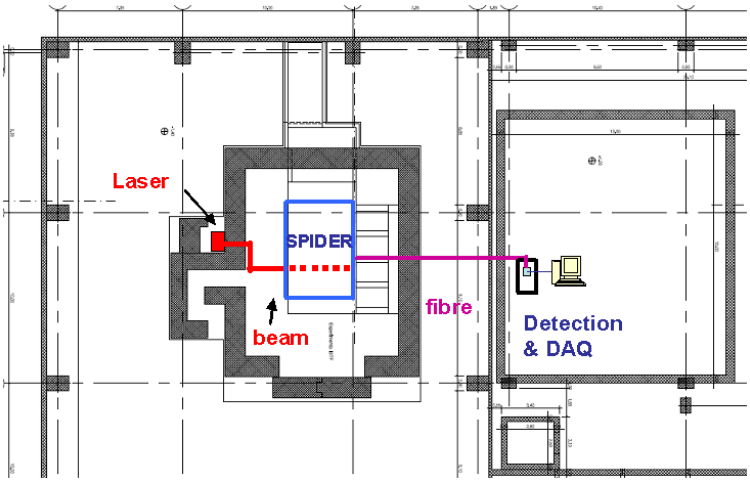

Figure 6. Plan view of the CRDS layout in the test facility building.

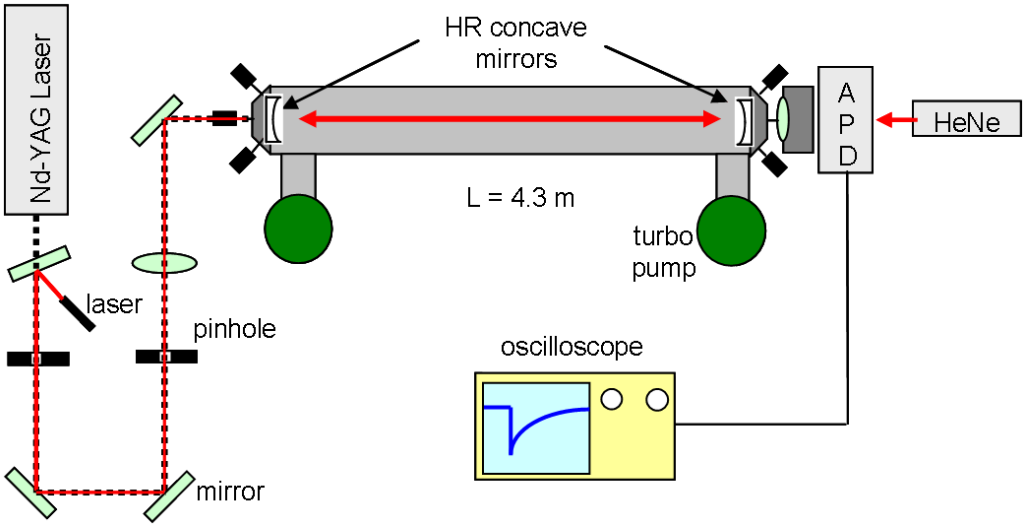

Figure 7. Schematic layout of the prototype CRDS system for SPIDER.

The two cavity mirrors have radius of curvature $r = 6\,\mathrm{m}$ to obtain a stable cavity and nominal reflectivity $R > 99.998\%$. In such a cavity the fundamental mode has a diameter of 1 mm across the path, which will also be the spatial resolution perpendicularly to the grid, but other modes can develop with larger diameter, especially if the cavity is not perfectly aligned and certainly they are present at the initial round trips, soon after the beam pulse enters the cavity, till they extinguish.

Alignment is performed with three fine pitch screws on each mount, whose sensitivity is just enough, because turning 15° the screw, which corresponds to 2.8 mm lateral shift at the opposite end of the cavity, is sufficient to completely miss the signal. The alignment procedure employs two co-aligned visible laser beams counter propagating through the cavity and uses a pinhole at the opposite end of each mirror to be aligned. Few iterations are sufficient to see a signal, collected through a focusing lens by an avalanche photodiode (APD). The APD has 3 mm diameter active

2012 JINST 7 C04016

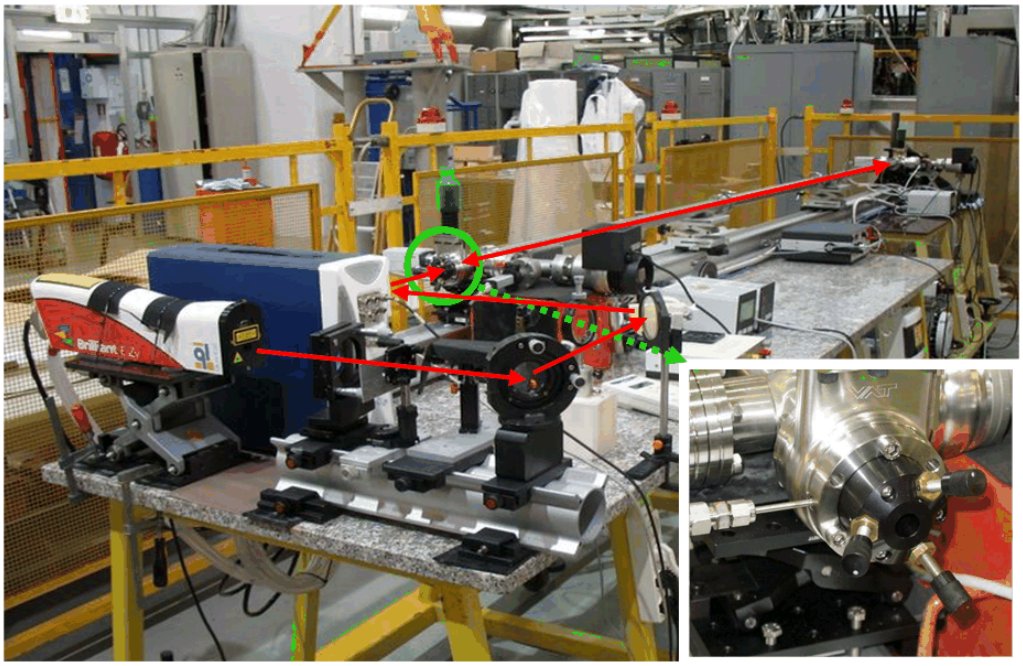

Figure 8. Photograph of the prototype CRDS system for SPIDER, with overlapped the beam path. In the zoomed section, the conflate flange that serves as cavity mirror mount: the three fine pitch screws used for mirror alignment are visible, at 120° from each other.

area, 40 MHz bandwidth and 3×10^5 V/A total transimpedance gain. In this test the signal is recorded by an 8 bit, 3GS/s oscilloscope, but in the SPIDER setup a digitiser with 12 bit and 250 MS/s will be used.

At optimum alignment a clean exponential decay is observed, modulated by the train of pulses escaping the cavity, which are distinguishable because of the long cavity and the high detection/acquisition bandwidth: the detected laser pulse duration is in fact 20 ns FWHM to be compared to a round trip time of 29 ns (figure 9). Fitting the signal with an exponential, fit residuals indicate deviations at the beginning of the decay, because multiple modes develop and overlap, quickly extinguishing, and at the end, where the signal is too small. A reference ring down time $\tau_0 = 82\,\mu$s was obtained by fitting the central part of the signal, independently from using the modulated raw signal or low-filtering it at 5 MHz to remove the oscillations. This τ_0 value corresponds to a mirror reflectivity $R = 99.98\%$. Uncertainty on τ_0 was not dominated by the standard deviation of the fit, which is just 0.1%, but by shot-to-shot random variations of about 6%. This variation can be reduced by averaging over multiple pulses. Its origin is not clear yet, but it might be caused by the laser pointing stability. However, measurements repeated after several months with the same setup have shown a random variation five times smaller ($\sim 1\%$), around the same value of τ_0, which indicates that the mirrors did not deteriorate.

The expected accuracy of the H^- density measurements has been calculated as a simple error propagation from (4.3), by considering $\sigma_\tau = \sigma_{\tau_0} = 1.2\,\mu$s (equivalent to 1.5% of the measured τ_0), not dependent on τ. Figure 10 reports the result as a function of the H^- density, together with the calculated ring down time, based on the measured τ_0. Three cases have been reported: single pulse

2012 JINST 7 C04016

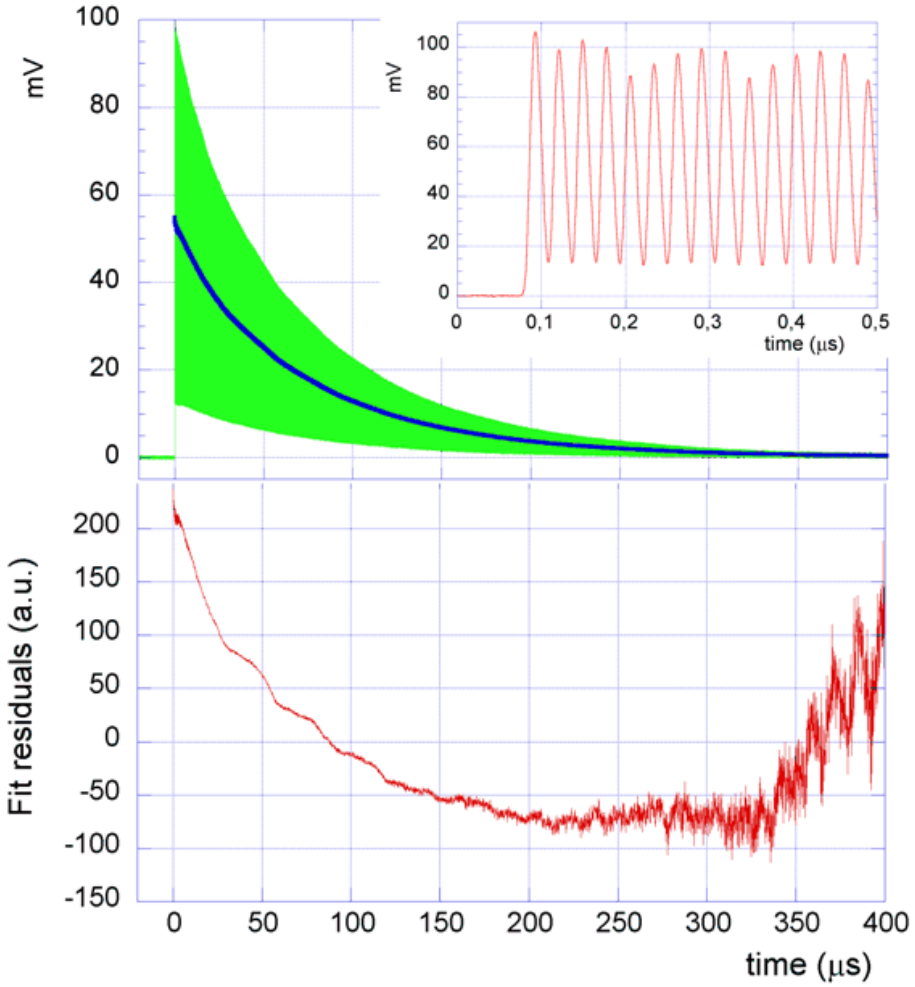

Figure 9. *Top*: measured reference CRDS signal: the line represents the filtered signal; in the box a zoom of the beginning of the decay, showing that the exponential is modulated by oscillations corresponding to the pulse round trip, but also with other spectral contributions at lower frequency. *Bottom*: residuals of the exponential fit.

measurement and average of 10 or 30 consecutive pulses, thus reducing the effective repetition rate from 10 Hz single pulse to 1 or 0.3 Hz respectively. Averaging brings the benefit of reducing the standard deviation and extending the operational range, represented by the density range with standard deviation below the target maximum value of 20%, so that density variations down to few 10^{15} m^{-3} can be discriminated.

When alignment deteriorates, the complex mode structure develops and eventually dominates, destroying the exponential behaviour. A spectral analysis of the signal, at optimised alignment, at three different phases of the decay, shows that at the beginning, in addition to the stable peak at 35 MHz, corresponding to the ring down frequency, additional peaks at lower frequencies appear, compatible with beating of different transverse modes or to intermodulation of modes (figure 11). In order to distinguish beats from transverse modes, the cavity length was reduced from 4.30 m to 2.72 m. The CRDS signal with this new layout is reported in figure 12, where the round trip

2012 JINST 7 C04016

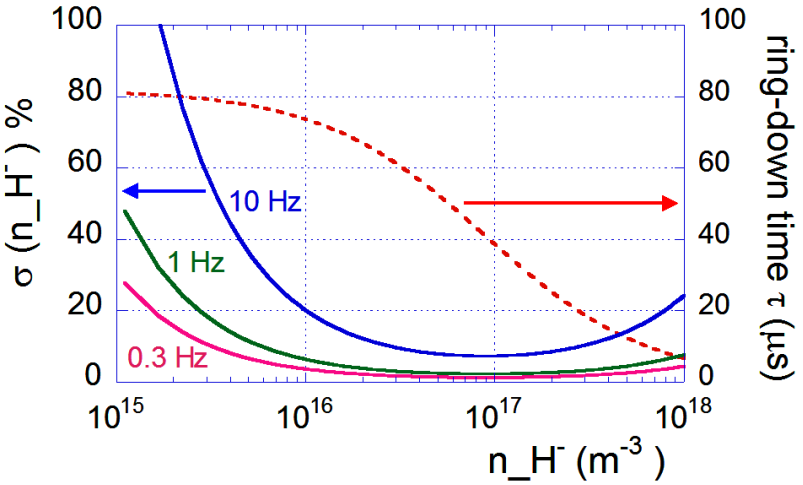

Figure 10. Ring-down time (dashed line) and expected relative standard deviation of H^- density (full lines) vs H^- density.

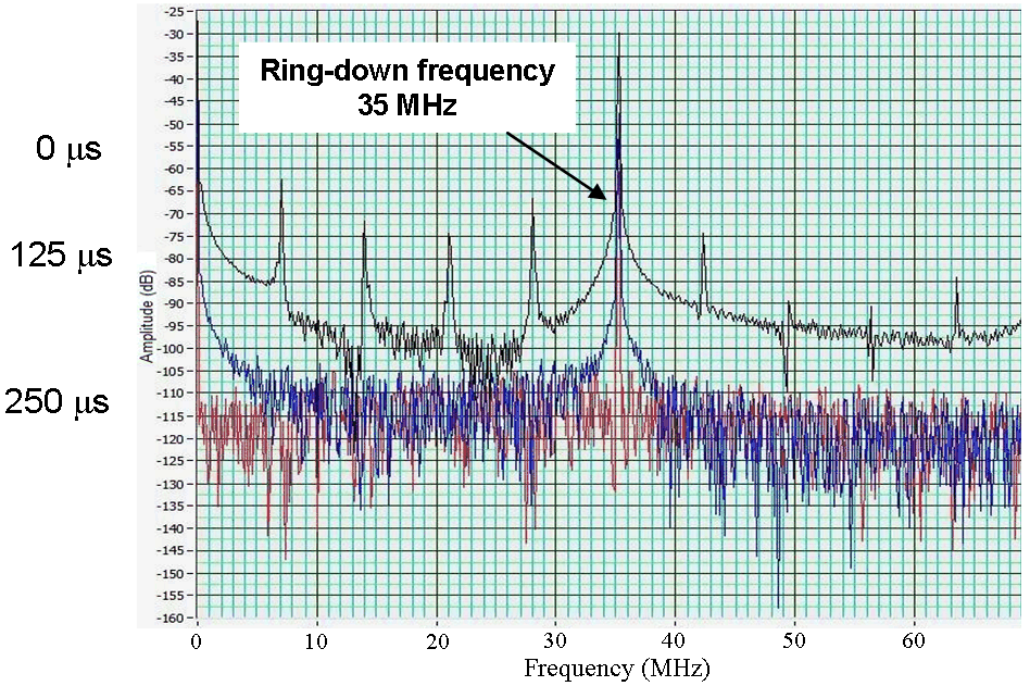

Figure 11. Spectral analysis of signal in figure 9, at three different times along the exponential decay: 0 μs (black curve) i.e. just after the laser pulse, 125 μs (blue) and 250 μs (red). Clearly the complex mode structure appears only at the beginning of the decay.

oscillation is much less apparent, while the new spectrum in figure 13 now shows distinguishable beats and transverse modes.

Real time acquisition and simple analysis between laser pulses at 10 Hz has been demonstrated on a PC. Each acquired waveform (10^5 samples at 200 MS/s) first is background subtracted, then filtered to remove oscillations (not necessary if a detector with lower bandwidth is used instead);

2012 JINST 7 C04016

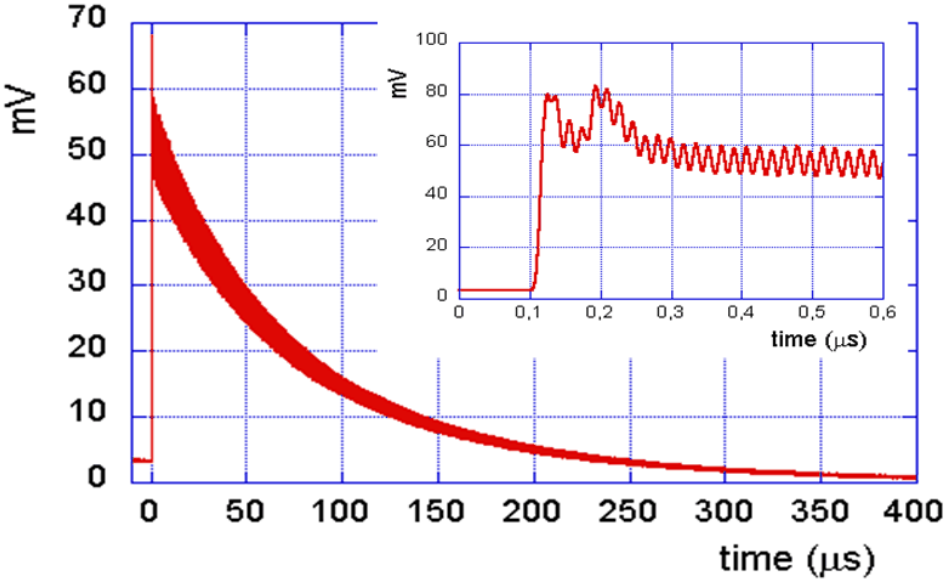

Figure 12. CRDS signal with reduced cavity length ($d = 2.72$ m).

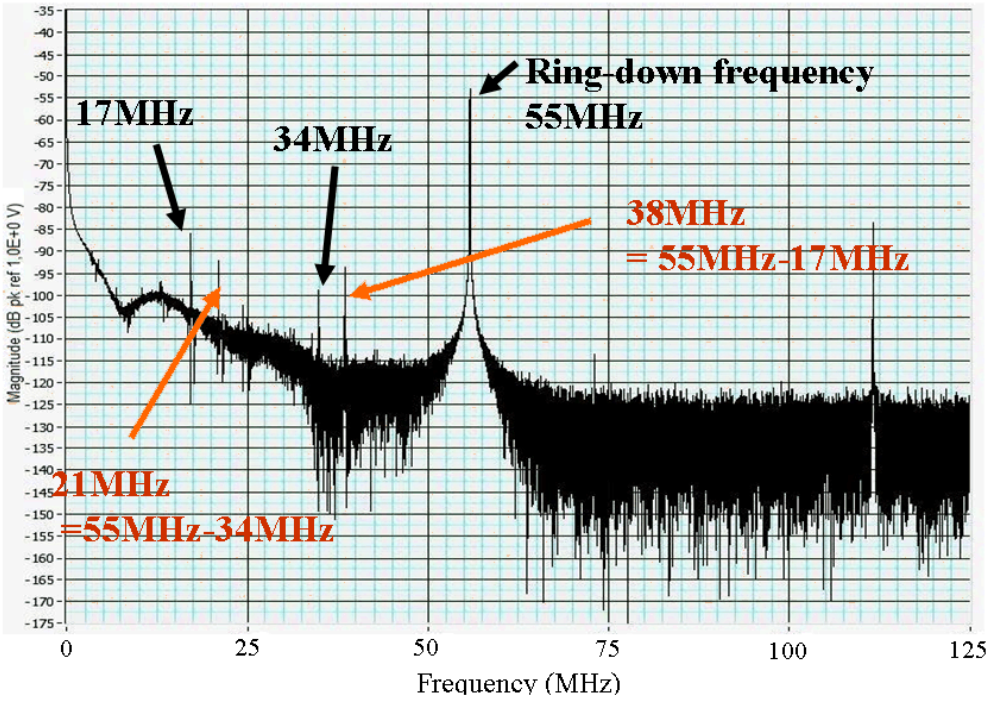

Figure 13. Spectral analysis of signal in figure 12.

the clean central part of the exponential is extracted and linearly fit in logarithmic scale; data are finally stored to disc.

Tests have been repeated at delays of months both with the same APD and replacing it with other detectors: photodiodes with 1 mm and 2 mm diameter active area, either directly coupled

2012 JINST 7 C04016

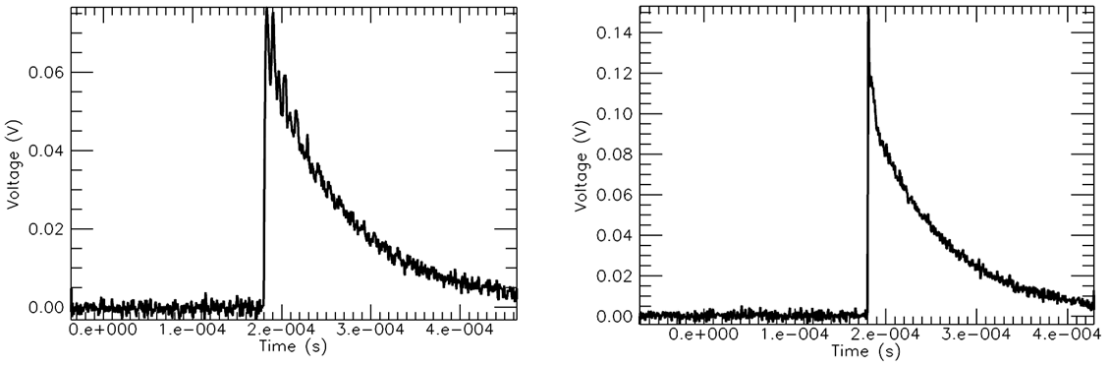

Figure 14. Filtered CRDS signals measured with 1 mm (*left*) and 2 mm (*right*) diameter photodiodes, directly coupled to the cavity through a lens.

to the cavity with a lens or through a 1 mm diameter optical fibre. In all cases photodiodes were amplified at 10^7 V/A with a bandwidth ranging from 50 to 400 kHz. It was found that, after major realignments or detector change, τ_0 could vary by microseconds, from 82 to 91 μs. As illustrated in figure 14, measurements with the 1 mm photodiode show a weak multimode pattern, which is an indication that not all the beam footprint is collected by the detector. However its effect was not so bad, as the estimated τ_0 was not significantly different from the values obtained with the APD. The 2 mm photodiode, maybe because of the larger active area, obtained a higher signal and a cleaner exponential decay. These last tests can however be improved in terms of mechanical setup, which was not optimised. Changing bandwidth in the available range did not vary significantly τ_0, however a larger bandwidth is required when τ will decrease down to 20–30 μs because of H^- absorption.

To summarise, experience on the benchtop prototype has validated the main characteristics and components of the CRDS design for SPIDER. In particular it has shown that alignment of such a long cavity is just feasible with the selected cavity mirror mounts, but an improved solution would be preferable, and has allowed to develop an alignment procedure. The multimode structure at the beginning of the decay is disturbing but it does not threat the measurement. A more subtle problem could be the random variation of the decay time, especially if the interval of variation will change in time. Finally, it has been shown that coupling of the 1 mm diameter fibre to the cavity might be critical because of the small diameter and will certainly require a lens and a careful mechanical design.

5 Laser absorption spectroscopy

H^- surface production is mainly influenced by the work function of the cesiated PG surface, which likely has a spatial dependence. However the work function is practically impossible to measure in the source, but only in dedicated ad hoc experimental setups [4], so that efforts have focused so far on measuring the cesium density near the converter surface. Cesium is more than 90% ionised during a plasma discharge, but emission lines of cesium ions are in the far UV (70–93 nm), and thus difficult to detect [17]. Normally the relative line integrated neutral cesium density is evaluated instead, near the PG, by measuring the emission line at 852.1 nm. This is possible only during

the plasma phase, while cesium evaporation and dynamics during the vacuum phase between the plasma pulses is important to the cesium layer build up.

Laser absorption spectroscopy has been pioneered at IPP RF ion sources to measure the cesium density also during the vacuum phase [17–19], proving to be very useful, easy to implement and operate.

The same resonance transition used by emission spectroscopy is chosen, which, considering the hyperfine structure and the Doppler broadening, results into two measured lines separated by 21.4 pm. The experimental setup at IPP [17] consists of a 150 mW tuneable, single mode, fibre coupled, distributed feedback diode laser, with 0.01 pm linewidth. The beam from the fibre is collimated to 11.5 mm diameter before entering the source and focused into a fibre after passing the source. Finally the signal is detected by an amplified photodiode, so that only optical components need to be installed inside the bioshield. The sensitivity range is 10^{13}–10^{17} m^{-3}, with 100 ms temporal resolution.

The ground state density can be directly calculated from:

$$n_k = \frac{8\pi c}{\lambda_0^4} \cdot \frac{g_k}{g_i} \cdot \frac{1}{A_{ik} l} \cdot \int_{\text{line}} \ln\left(\frac{I(\lambda, l)}{I(\lambda, 0)}\right) d\lambda \tag{5.1}$$

where g_i and g_k are the statistical weight of upper and lower level, A_{ik} the Einstein transition probability for spontaneous emission, $I(\lambda, 0)$ the injected spectral intensity and $I(\lambda, l)$ the same quantity after passing through a length l of absorbing medium. Data evaluation needs however to consider two saturation effects: line saturation and depopulation of the ground state density [17].

Typical cesium density of about 10^{15} m^{-3} in the vacuum phase was measured at IPP sources. The beneficial effect of controlling the surface temperature has been seen using this diagnostic: an improved cesium redistribution is obtained also after evaporation is switched off. Signal evolution before, during and after a plasma discharge, shows a complex behaviour and its analysis needs to take into account that a large fraction of the cesium neutrals are ionized during the discharge and recombine after it. It is found that the signal during the discharge is, after few conditioning discharges, similar to that in the vacuum phase, even though a decrease would be expected, but this can be explained by a large release of cesium from the wall during the discharge. When the plasma is switched off, a strong peak appears, caused by recombination of ionized cesium, followed by an exponential decay caused by transport to the wall [19].

The laser absorption diagnostic will be installed in SPIDER, by applying a design similar to that used in the IPP sources. The layout will be very similar to that of the CRDS system, with the laser outside the bioshield and the detection and acquisition systems in a separate room. It can use the same set of horizontal LOSs designed for emission spectroscopy and CRDS; by splitting the beam over multiple LOSs, the measurements at different heights over the grid can be simultaneously measured and compared, providing information on the spatial uniformity. SPIDER will operate with long pulses, where laser absorption can usefully complement the measurement of the 852 nm emission line, because the latter is influenced by the evolution of the plasma parameters that contribute to the signal, while the former is independent from them, as observed in [19].

2012 JINST 7 C04016

6 Conclusion

CRDS and laser absorption spectroscopy diagnostics are being developed for the SPIDER RF source. CRDS advanced design has been already tested on a prototype, while laser absorption spectroscopy is still at an earlier stage. Both designs are based on the positive experience gained at smaller sources at IPP Garching. Design finalization of the two diagnostics will take advantage of continuing operation of existing systems at IPP and NIFS and experimental optimization will be carried out, before installation on SPIDER, also through operation on the small RF source NIO, under construction at Consorzio RFX [20].

Acknowledgments

This work was set up in collaboration and financial support of Fusion for Energy. Author thanks the negative neutral beam team at IPP Garching, particularly U. Fantz and C. Wimmer, and H. Nakano of NIFS, Japan, for fruitful discussions on their diagnostics and results. Thanks also to Marco Barbisan, who has contributed to assembly and test the CRDS prototype for SPIDER.

References

[1] R. Hemsworth et al., *Status of the ITER heating neutral beam system*, *Nucl. Fusion* **49** (2009) 045006.

[2] P. Sonato et al., *The ITER full size plasma source device design*, *Fusion Eng. Des.* **84** (2009) 269.

[3] U. Fantz et al., *Physical performance analysis and progress of the development of the negative ion RF source for the ITER NBI system*, *Nucl. Fusion* **49** (2009) 125007.

[4] R. Gutser, C. Wimmer and U. Fantz, *Work function measurements during plasma exposition at conditions relevant in negative ion sources for the ITER neutral beam injection*, *Rev. Sci. Instrum.* **82** (2011) 023506.

[5] G. Serianni, N. Pomaro, R. Pasqualotto, M. Spolaore and M. Valisa, *The diagnostic system of the neutral beam injectors for ITER heating and current drive*, *Rev. Sci. Instrum.* **79** (2008) 10F307.

[6] R. Pasqualotto et al., *Diagnostics of the ITER neutral beam test facility*, in Book of Abstracts of the *14th International Conference on Ion Sources*, Giardini Naxos Italy, 12–16 Sep 2011, *Rev. Sci. Instrum.* **83** (2012) 02B103.

[7] R. Pasqualotto et al., *Spectroscopic diagnostics for the negative ion RF source SPIDER*, *Nucl. Instrum. Meth.* **A 623** (2010) 794.

[8] G. Berden and R. Engeln, *Cavity ring-down spectroscopy*, John Wiley & Sons Inc., New York U.S.A. (2009).

[9] F. Grangeon et al., *Applications of the cavity ring-down technique to a large-area rf-plasma reactor*, *Plasma Sources Sci. Technol.* **8** (1999) 448.

[10] M. Berger, U. Fantz, S. Christ-Koch and NNBI Team, *Cavity ring-down spectroscopy on a high power rf driven source for negative hydrogen ions*, *Plasma Sources Sci. Technol.* **18** (2009) 025004.

[11] H. Nakano et al., *Cavity ring-down system for density measurement of negative hydrogen ion on negative ion source*, *AIP Conf. Proc.* **1390** (2011) 359.

2012 JINST 7 C04016

[12] H. Nakano et al., *Negative-hydrogen-ion density measurement in beam extraction region of large-scaled source for neutral beam injector*, in Book of Abstracts of the *14th International Conference on Ion Sources*, Giardini Naxos Italy, 12–16 Sep 2011, http://icis11.lns.infn.it/BoA.pdf.

[13] M. Bacal, *Photodetachment diagnostic techniques for measuring negative ion densities and temperatures in plasmas*, *Rev. Sci. Instrum.* **71** (2000) 3981.

[14] U. Fantz and D. Wünderlich, *A novel diagnostic technique for H^- (D^-) densities in negative hydrogen ion sources*, *New J. Phys.* **8** (2006) 301.

[15] S. Christ-Koch, U. Fantz, M. Berger and NNBI Team, *Laser photodetachment on a high power, low pressure rf-driven negative hydrogen ion source*, *Plasma Sources Sci. Technol.* **18** (2009) 025003.

[16] R. Pasqualotto, A. Alfier and L. Lotto, *Design of a CRDS diagnostic for negative ion RF source SPIDER*, *Rev. Sci. Instrum.* **81** (2010) 10D710.

[17] U. Fantz and C. Wimmer, *Optimizing the laser absorption technique for quantification of cesium densities in negative hydrogen ion sources*, *J. Phys.* **D 44** (2011) 335202.

[18] U. Fantz, C. Wimmer and NNBI Team, *Quantification of cesium in negative hydrogen ion sources by laser absorption spectroscopy*, *AIP Conf. Proc.* **1390** (2011) 348.

[19] U. Fantz and C. Wimmer, *Cesium dynamics in long pulse operation of negative hydrogen ion sources for fusion*, in Proceedings of the *14th International Conference on Ion Sources*, Giardini Naxos Italy, 12–16 Sep 2011, *Rev. Sci. Instrum.* **83** (2012) 02B110.

[20] M. Cavenago et al., *Development of a versatile multiaperture negative ion source*, in Book of Abstracts of the *14th International Conference on Ion Sources*, Giardini Naxos Italy, 12–16 Sep 2011, *Rev. Sci. Instrum.* **83** (2012) 02A707.

2012 JINST 7 C04016